Journal of Power Sources 196 (2011) 1042–1047

Contents lists available at ScienceDirect

Journal of Power Sources

journal homepage: www.elsevier.com/locate/jpowsour

Investigation of carbon supported Au–Ni bimetallic nanoparticles as electrocatalyst for direct borohydride fuel cell

Peiying He [a], Ying Wang [b], Xianyou Wang [a,*], Fu Pei [a], Hong Wang [a], Li Liu [a], Lanhua Yi [a]

[a] Key Laboratory of Environmentally Friendly Chemistry and Applications of Ministry of Education, School of Chemistry, Xiangtan University, Hunan 411105, China
[b] School of Chemical Engineering and Pharmacy, Wuhan Institute of Technology, Hubei, Wuhan 430073, China

ARTICLE INFO

Article history:
Received 16 July 2010
Received in revised form 12 August 2010
Accepted 13 August 2010
Available online 19 August 2010

Keywords:
Direct borohydride-hydrogen peroxide fuel cell
Au–Ni bimetallic nanoparticles
Electrocatalyst
Cell performance

ABSTRACT

The carbon supported $Au_{80}Ni_{20}$, $Au_{58}Ni_{42}$ and $Au_{41}Ni_{59}$ nanoparticles for the application of direct borohydride-hydrogen peroxide fuel cell (DBHFC) are synthesized in a sodium bis(2-ethylhexyl) sulfosuccinate (AOT) reverse micelle system. The physical and electrochemical properties are investigated by transmission electron microscopy (TEM), cyclic voltammetry, chronoamperometry, chronopotentiometry and fuel cell test. The TEM results reveal that the Au–Ni bimetallic particles are uniformly dispersed on carbon with narrow size distribution and regular spherical shape. The average size of the particles is about 3 nm. The electrochemical measurements show that Au–Ni bimetallic particles can apparently promote the electrode kinetics of BH_4^- oxidation. The DBHFCs using carbon supported Au–Ni bimetallic particles as anode electrocatalysts are fabricated. The results show that the performance of DBHFC using $Au_{58}Ni_{42}$/C as anode electrocatalyst excels markedly to the others, and the maximum power density of 45.74 mW cm^{-2} is obtained at 20 °C.

1. Introduction

The proton exchange membrane fuel cell (PEMFC), using hydrogen as fuel, is the most advanced fuel cell today because of their high energy conversion efficiency and environmental friendliness. However, there still remain some problems, among which transportation and storage of hydrogen is one of the biggest. Direct sodium borohydride fuel cell (DBFC) is another attractive choice without hydrogen transportation and storage problems because borohydride is used as reactant directly in the fuel cell [1–7]. This type of fuel cell has many advantages. For example, the sodium borohydride is non-toxic, high hydrogen content (weight content of 10.6%) and high capacity (5.7 Ah g^{-1}). The anode reaction in an aqueous alkaline medium according to an eight-electron process is described as following [8].

$$BH_4^- + 8OH^- \rightarrow BO_2^- + 6H_2O + 8e^-, \quad E^0 = -1.24\,V \text{ vs. SHE} \quad (1)$$

However, on the most of metals and alloys studied in relation to BH_4^- oxidation, the complete 8e$^-$ exchange is not achieved due to hydrolysis of borohydride according to Eq. (2) [9–11].

$$BH_4^- + xOH^- \rightarrow BO_2^- + (x-2)H_2O + (4-(1/2)x)H_2 + xe^- \quad (2)$$

It was well reported that high coulombic numbers near 8e$^-$ were obtained by using Au anodes due to its inactivity towards the hydrolysis reaction [4,12–14]. However, the Au electrode usually demonstrates slow electrode kinetics and thus low current and power output [11].

From the view of fuel cell power output in the literatures, fast electrode kinetics and outstanding power performances were obtained on Ni, Pt and Pd [11,15–18]. Usually, the catalyst cost of fuel cell is a main factor limited its application. Ni catalyst as a non-noble metal and high power output may be worthwhile to be studied for the application of DBFC. It is well known that bimetallic catalysts systems often show higher catalytic activity and better stability than the monometallic systems [19,20]. The Au-bimetallic with non-noble metal such as Ni can reduce the cost of catalyst, and keep or even improve the catalytic activity for the direct oxidation of BH_4^- and power output. But, to the author's knowledge, carbon supported Au–Ni bimetallic particles have been less reported as anode catalysts for the DBFC.

In our previous studies, carbon supported hollow gold nanoparticles were prepared and used as the anodic catalyst of DBFC, the cell output power is clearly improved [21]. In this study, a series of carbon supported Au–Ni bimetallic nanoparticles were prepared by a reverse micelle method and their electrocatalytic activity with respect to BH_4^- oxidation were studied by both fundamental electrochemical techniques and fuel cell experiments.

* Corresponding author. Tel.: +86 731 58292060; fax: +86 731 58292061.
E-mail address: wxianyou@yahoo.com (X. Wang).

0378-7753/$ – see front matter © 2010 Elsevier B.V. All rights reserved.
doi:10.1016/j.jpowsour.2010.08.037

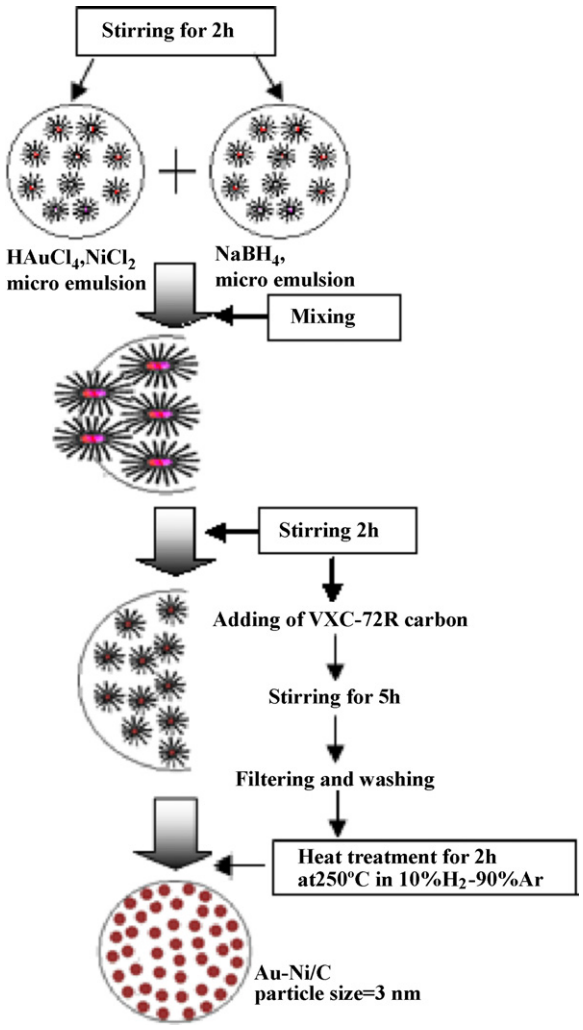

Fig. 1. The preparation process sketch of Au–Ni bimetallic nanoparticles.

2. Experimental

2.1. Preparation of carbon supported Au–Ni nanoparticles

Au–Ni bimetallic nanoparticles were prepared in an AOT reverse micelle system. Fig. 1 illustrates the preparation process sketch of Au–Ni nanoparticles highly dispersed on carbon support based on a reverse micelle method. Briefly, a stock solution of 0.10 M AOT/*n*-heptane was first made up. Then, two sets of reverse micelle solutions were prepared by injecting equal amounts of aqueous stock solutions of metal salts ($HAuCl_4$, $NiCl_2$) or sodium borohydride to give the required $w_0 (w_0 = 5)$, which is defined as the molar ratio $[H_2O]/[AOT]$ in the reverse micelle solutions. The two sets of reverse micelle solutions were mixed after stirring independently for 2 h. The mixture was kept under stirring for 2 h. Subsequently, appropriate content Vulcan XC-72R carbon was added to the above solution and stirred for another 5 h. The powder was dried at 80 °C for 24 h in a vacuum after filtrated and washed. Finally, the catalyst powder was mildly heat treated at 250 °C in a flowing mixture of 10% H_2 and 90% Ar. The atomic ratios of Au/Ni which contained in the reverse micelle solutions were 100:0, 75:25, 50:50 and 25:75. The prepared catalysts were marked as Au/C, AuNi/C-1, AuNi/C-2 and AuNi/C-3, respectively.

Table 1
Atomic ratios of as-prepared four catalysts.

Catalysts	Initial composition Au:Ni (atomic ratio)	Composition from EDX Au:Ni (atomic ratio)
AuNi/C-1	75:25	80:20
AuNi/C-2	50:50	58:42
AuNi/C-3	25:75	41:59

2.2. Characterization of Au–Ni/C electrocatalysts

The Au–Ni atomic ratios of Au–Ni/C catalysts were determined by energy dispersion X-ray (EDX) spectra analysis with the system attached to A JEOL model JSM-5600LV field emission transmission electron microscope. The structure and morphology of the Au–Ni/C electrocatalysts were examined by transmission electron microscopy (TEM) using a FEI Tecnai G2 microscope.

2.3. Electrochemical measurements

The Au–Ni/C working electrode was prepared as follows: 10 mg Au–Ni/C electrocatalyst was dispersed by ultrasonic for 2 h in 1 ml solution composed of 0.25 ml 5% Nafion solution and 0.75 ml distilled water. Then 5 μl of suspension was carefully applied on glass carbon (GC) (3 mm in diameter) electrode surface. The dispersed Au–Ni/C electrocatalyst on the GC surface was dried at room temperature. The loading mass of Au/C or Au–Ni/C electrocatalyst was 0.7 mg cm^{-2}.

A conventional three-electrode cell was used to perform the electrochemical tests. The cell was composed of the Au–Ni/C working electrode, a Pt foil with 1 cm^2 as counter electrode and an Ag/AgCl (3 M KCl) via a Luggin capillary with a salt bridge as the reference electrode. Cyclic voltammetry, chronoamperometry and chronopotentiometry experiments were conducted with a CHI660A Electrochemistry Workstation.

2.4. Fuel cell test

The cell design and electrode preparation procedure were shown in our previous report [21]. A small compartment cell was used in which the activated Nafion 117 membrane was compressed between the two halves. Solution was then poured into both sides of the cell, 3 M NaOH + 1 M $NaBH_4$ on the anode side and 0.5 M H_2SO_4 + 2 M H_2O_2 on the cathode side. The load was applied in steps of 5 mA within the range of 0–120 mA. Each step lasted 2 min and the current was continuously applied from one value to the next without disconnecting the cell. All cell tests were carried out at 20 °C. The anode and cathode were a piece of stainless steel gauze coated in Au–Ni/C and Au/C (4.5 mg cm^{-2}), respectively.

3. Results and discussion

3.1. Physical characterization of the carbon supported electrocatalysts

The results of EDX analysis for the carbon supported electrocatalysts are shown in Table 1. According to Table 1, AuNi/C-1, AuNi/C-2 and AuNi/C-3 are responded to $Au_{80}Ni_{20}/C$, $Au_{58}Ni_{42}/C$ and $Au_{41}Ni_{59}/C$, respectively. Apparently, the Au–Ni atomic ratios found from EDX analysis are not very similar to the originally inputs. The deviation of composition among three bimetallic catalysts might be caused by three reasons. Firstly, the standard reduction potential of the Ni^{2+}/Ni redox pair (−0.257 V vs. SHE) is much lower than that of the $AuCl_4^-/Au$ redox pair (0.994 V vs. SHE). Not all the Ni^{2+} in nanoparticles can be completely reduced. Secondly, during the course of reaction, part of the Ni in the resul-

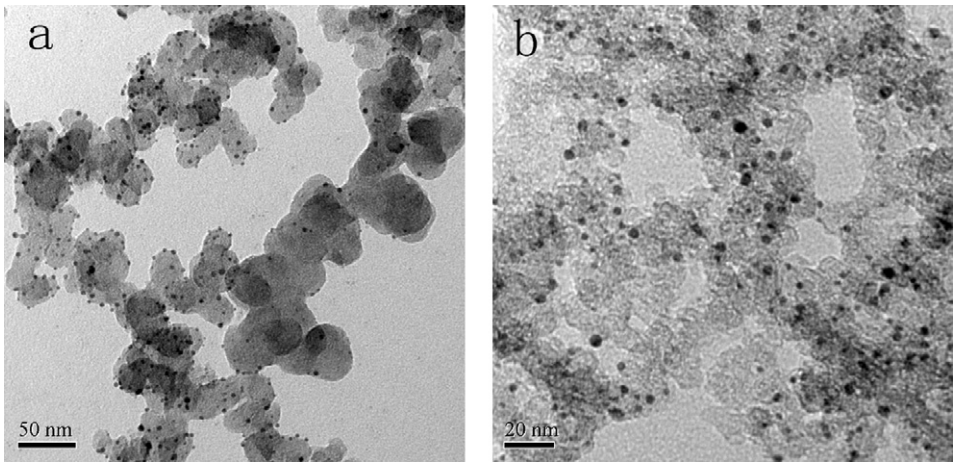

Fig. 2. TEM images of $Au_{58}Ni_{42}$ nanospheres dispersed on carbon.

tant Au–Ni bimetallic nanoparticles were oxidized to Ni^{2+}, and thus resulting in that the real content of Ni in Au–Ni/C catalysts is lower than the theoretical value. Finally, the deviation of composition might be caused by detection errors because the particles were too fine and the low number of particles chosen for analysis.

The morphology and distribution of catalysts were observed by TEM. Because the preparation methods of Au–Ni/C catalysts were identical, the morphology and structure of as-prepared Au–Ni/C catalysts were similar, so $Au_{58}Ni_{42}$/C catalyst was chosen as the representative to analysis. Fig. 2 shows TEM images of $Au_{58}Ni_{42}$/C catalyst. It was found that Au–Ni bimetallic nanoparticles were evenly distributed throughout carbon black with fairly narrow size distribution, and the average diameter is approximately 3 nm. Such an excellent size-controlling is one of the great advantages for preparing nanoparticles through a reverse micelle method. Because the metal catalyst particles were formed by the reduction of metal precursor(s) at the limited space in each nanocapsule, the particle size could be settled into such a narrow size distribution.

3.2. Electrochemical catalyst surface characterization

As a surface sensitive technique, the cyclic voltammetry was applied to obtain the surface composition and characteristic of the catalysts according to the zone of surface oxide reduction. Fig. 3 presents cycle voltammograms recorded in deaerated 3.0 M NaOH electrolyte at the Au/C and Au–Ni/C catalysts. It is seen that the cyclic voltammogram of Au/C electrocatalyst shows a typical voltammetric response of Au surface in alkaline condition [22]. Au-oxide was formed at 0.28 V vs. Ag/AgCl (0.5 V vs. NHE) at the positive scan and reduced at −0.02 V vs. Ag/AgCl (0.2 V vs. NHE) at the negative scan. The Au–Ni/C electrodes also show the characteristic features of Au surface electrochemistry. Besides, the Au–Ni/C electrodes appear a pair of redox peaks in the potential range of 0.2–0.5 V vs. Ag/AgCl, which correspond to the oxidation–reduction of nickel hydroxide ($Ni(OH)_2$). However, the intensity of the peak current around 0 V vs. Ag/AgCl with respect to oxide stripping on Au are different from the intensity of the peak current around 0.23 V with respect to hydroxide stripping on Ni. This phenomenon indicates that the amounts of exposed Au sites and Ni sites on the surface of Au–Ni/C catalysts are different, which may be caused by the different reduction rates of Au and Ni ions.

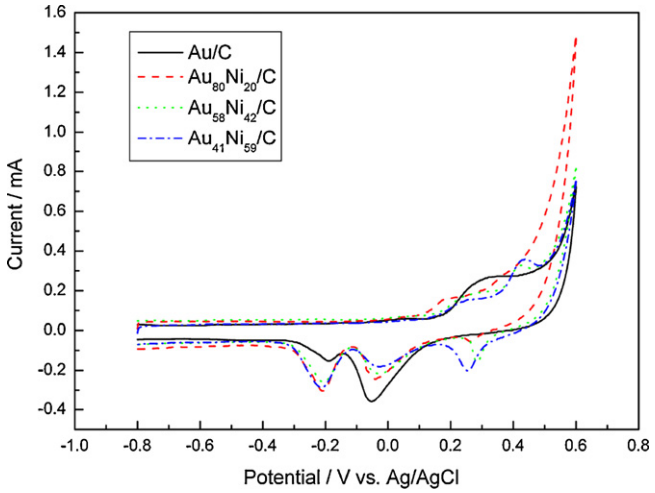

Fig. 3. Cyclic voltammograms of Au/C and Au–Ni/C electrodes in 3.0 M NaOH at a sweep rate of 50 mV s^{-1}.

Finally, the Au and Ni electroactive surface areas in the catalysts are calculated by the charge associated with the Au surface oxide stripping peak (420 μC cm^{-2}) [23] and the Ni surface oxidation reduction peak (514 μC cm^{-2}) [24–26], respectively. Using the radii and FCC crystal lattice parameters of Au and Ni, the ratio of their electroactive surface areas can evaluate the atomic composition of the Au–Ni electrode surfaces. Results are collected in Table 2. The ratios of (electroactive) atomic composition Au:Ni, are much higher than the results of EDX analysis, indicating the surface is Au-rich for Au–Ni alloys. The Au surface segregation in Au–Ni bimetallics is based on the higher mobility of Au atoms [27–29].

3.3. Cyclic voltammetry

With the aim to highlight the Au/C and Au–Ni/C electrocatalysts behaviours in $NaBH_4$ aqueous solution, we subtracted the voltammogram in 0.05 M $NaBH_4$ + 3.0 M NaOH by those in 3.0 M NaOH (Fig. 4 inset). The current density was normalized in reference to the Au weight for each catalyst. Thus, it can be directly compared for the catalytic activity of different catalysis. The background-corrected CV curves (inset) in Fig. 4b–d are similar to that observed in Au/C electrode (Fig. 4a). In the positive potential sweep, all curves have a strong oxidation current peak (a2), which has been previously reported in the literature and can be attributed to the direct, potentially eight-electron, oxidation of BH_4^- [13]. In the reverse potential sweep, a peak (c1) observed at 0.2 V vs. Ag/AgCl can be attributed to an absorbed species such as BH_3OH^- or other borohydroxides formed as an intermediate during the oxidation of BH_4^- [14]. Except for the same characterization, some especial phenomena are also obtained on Au–Ni bimetallic electrodes. As shown in

Table 2
The surface composition of Au/C and Au–Ni/C catalysts obtained by surface voltammetry.

Catalysts	Au/C	AuNi/C-1	AuNi/C-2	AuNi/C-3
Au electroactive surfaces/cm^2	0.15045	0.09464	0.08972	0.07745
Ni electreoactive surfaces/cm^2	0	0.00564	0.01634	0.03853
Electreoactive composition Au:Ni (atomic ratio)	–	12.5:1	4.1:1	1.5:1

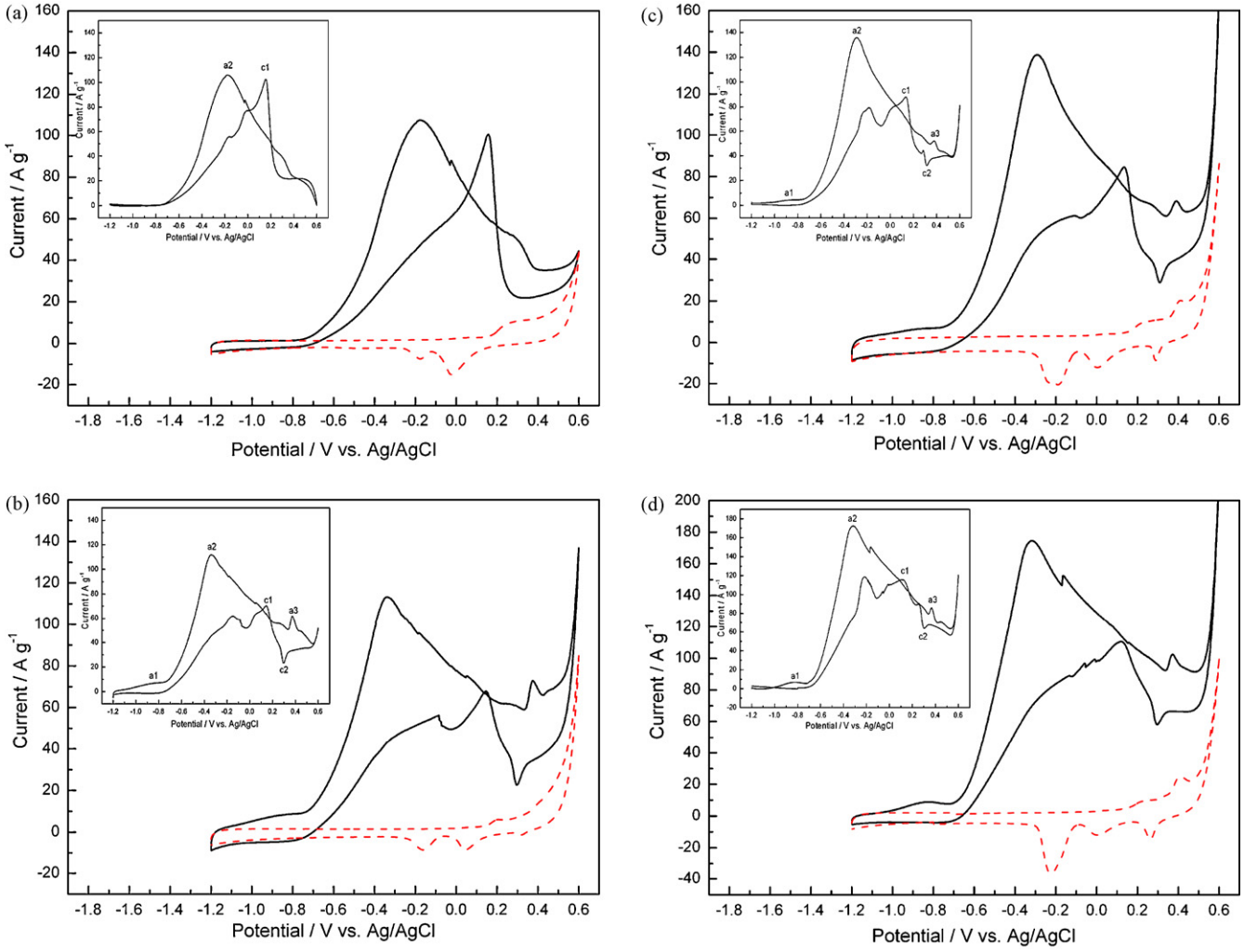

Fig. 4. Cyclic voltammogram (20 mV s^{-1}) plotted on (a) Au/C, (b) $Au_{80}Ni_{20}$/C, (c) $Au_{58}Ni_{42}$/C and (d) $Au_{41}Ni_{59}$/C in 3.0 M NaOH (dashed line) and in 3.0 M NaOH + 0.05 M $NaBH_4$ (solid line) and the corresponding subtraction results: 3.0 M NaOH + 0.05 M $NaBH_4$ − 3.0 M NaOH (inset) at 20 °C in argon atmosphere.

Fig. 4(inset)b–d, a oxidation peak (a1) between −1.0 V and −0.8 V vs. Ag/AgCl is due to the oxidation of H_2 generated by the catalytic hydrolysis of BH_4^- [19]. The hydrolysis mechanism of BH_4^- can be expressed as following:

$$NaBH_4 + yH_2O \rightarrow NaBH_{4-y}(OH)_y + yH_2, \quad y = 1, \ldots, 4 \tag{3}$$

$$(1/2)H_2 + OH^- \rightarrow H_2O + e^- \tag{4}$$

And a pair of redox peaks (a3 and c2) appears between 0.3 V and 0.5 V vs. Ag/AgCl, which correspond to the oxidation–reduction processes of nickel hydroxide.

$$Ni + 2OH^- \rightleftharpoons Ni(OH)_2 + 2e^- \tag{5}$$

The direct oxidation peak potentials and peak current densities of BH_4^- for Au/C and Au–Ni/C catalysts are summarized in Table 3. According to Table 3, the oxidation peak potentials of BH_4^- for Au–Ni/C catalysts are about 0.15 V more negative than the Au/C catalyst. It indicates that Au–Ni bimetallic nanoparticles can apparently improve the catalytic activity of Au and the electrode kinetics of BH_4^- oxidation. Although the content of Au in Au–Ni/C catalysts is less than that in Au/C, the peak current density at Au–Ni/C catalysts does not reduce; on the contrary, all the peak current density on the Au–Ni/C electrodes is higher than that on the Au/C electrode. It can be attributed to the synergistic effect of Au–Ni bimetallic nanoparticles. Au–Ni bimetallic nanoparticles jointly improve the electrochemical oxidation of BH_4^-. Among the four electrodes, the peak current density on the $Au_{41}Ni_{59}$/C electrode is the highest,

Table 3
The peak potential and peak current of BH_4^- on Au/C and Au–Ni/C catalysts.

Catalysts	Main peak potential (V)	Main peak current (A g^{-1})
Au/C	−0.175	105.76
$Au_{80}Ni_{20}$/C	−0.338	112.00
$Au_{58}Ni_{42}$/C	−0.298	135.97
$Au_{41}Ni_{59}$/C	−0.322	171.98

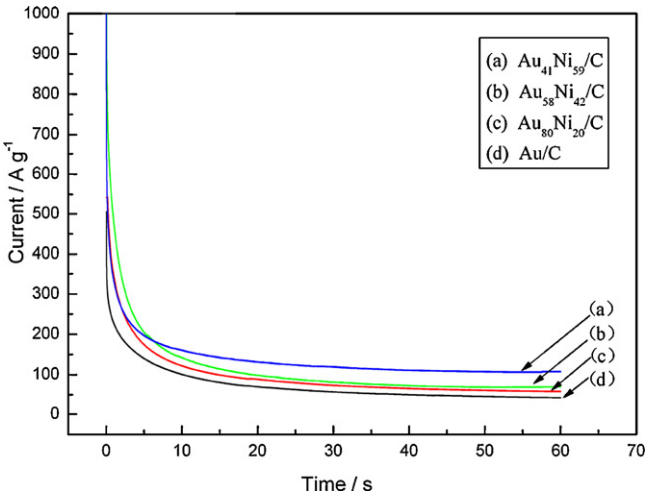

Fig. 5. Chronoamperometry curves of Au/C and Au–Ni/C electrodes in 0.1 M $NaBH_4$ + 3.0 M NaOH at 20 °C. Potential step from −1.0 V to −0.2 V vs. Ag/AgCl.

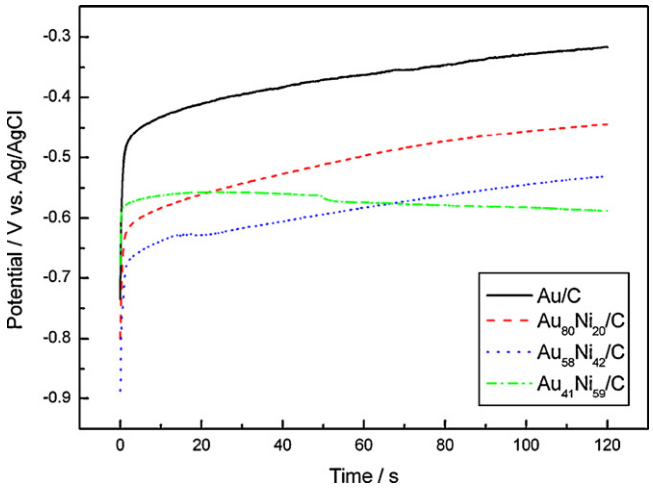

Fig. 6. Chronopotentiometry curves of Au/C and Au–Ni/C electrodes in 0.1 M $NaBH_4$ + 3.0 M NaOH at 20 °C. Current step was from 0 to 8.5 mA cm^{-2}.

which can be attributed to the $Au_{41}Ni_{59}$/C has the highest catalytic activity. But during the sweep, there were lots of gas bubbles generated on the surface of $Au_{41}Ni_{59}$/C electrode.

3.4. Chronoamperometry and chronopotentiometry

Fig. 5 shows the chronoamperometric response of the Au/C, $Au_{80}Ni_{20}$/C, $Au_{58}Ni_{42}$/C and $Au_{41}Ni_{59}$/C electrodes in 0.1 M BH_4^- solution in the case of a potential step from −1.0 V to −0.2 V vs. Ag/AgCl. As shown in Fig. 5, after 60 s, the current densities of Au/C, $Au_{80}Ni_{20}$/C, $Au_{58}Ni_{42}$/C and $Au_{41}Ni_{59}$/C are 43.78 A g^{-1}, 59.12 A g^{-1}, 70.93 A g^{-1} and 107.51 A g^{-1} (the current density was normalized in reference to the Au weight), respectively. It is indicated that the order of catalytic activity of four electrodes is Au/C < $Au_{80}Ni_{20}$/C < $Au_{58}Ni_{42}$/C < $Au_{41}Ni_{59}$/C.

Chronopotentiometry is a useful qualitative catalyst screening method since it simulates the constant current operation of a fuel cell [19]. Fig. 6 compares the chronopotentiogram of Au/C, $Au_{80}Ni_{20}$/C, $Au_{58}Ni_{42}$/C and $Au_{41}Ni_{59}$/C electrodes in a 0.1 M $NaBH_4$ + 3.0 M NaOH solution. It can be clearly seen from Fig. 6 that the overpotential of $Au_{41}Ni_{59}$/C was the smallest (about −0.588 V), followed by the $Au_{58}Ni_{42}$/C, $Au_{80}Ni_{20}$/C and Au/C. The overpotentials were −0.531 V, −0.444 V, and −0.317 V, respectively. A lower overpotential is an indication of better electroactivity. Among the four catalysts, with the increase of Ni contents, the overpotential of $NaBH_4$ oxidation decreases. These results indicate that Au–Ni bimetallic catalyst can apparently reduce the electrochemical polarization of BH_4^- at electrode reaction. The more is the Ni content, the less is the electrochemical polarization.

3.5. Cell performance

The $NaBH_4/H_2O_2$ fuel cell is a very promising candidate for a variety of small mobile power applications as well as for high power applications, especially for space or underwater use where oxygen is not readily available from air [6,30]. The electrode reactions and cell reaction can be described as following:

$$\text{Anode}: \quad BH_4^- + 8OH^- \rightarrow BO_2^- + 6H_2O + 8e^-, \quad E^0 = -1.24\,\text{V vs. SHE} \tag{6}$$

$$\text{Cathode}: \quad H_2O_2 + 2H^+ + 2e^- \rightarrow 2H_2O, \quad E^0 = 1.77\,\text{V vs. SHE} \tag{7}$$

$$\text{Cell reaction}: \quad BH_4^- + 2H_2O_2 \rightarrow BO_2^- + 6H_2O, \quad E^0_{cell} = 3.01\,\text{V} \tag{8}$$

The cell polarization and power density curves for direct borohydride-hydrogen peroxide fuel cell (DBHFC) operating with 1 M $NaBH_4$ + 3 M NaOH as fuel and 2 M H_2O_2 + 0.5 M H_2SO_4 as oxidant, while employing the Au/C as the cathode catalyst and Au/C, $Au_{80}Ni_{20}$/C, $Au_{58}Ni_{42}$/C or $Au_{41}Ni_{59}$/C as the anode catalyst, are presented in Fig. 7a and b, respectively. Main performance parameters of the DBHFC, such as open circuit voltages (OCVs) and power density on different anode catalysts are summarized in Table 4. According to Table 4, the OCVs values are about 1.8 V, which is lower than the theoretical value of DBHFC (3.01 V). This value probably represents a mixed potential at cathode [31]. As shown in Fig. 7a, the cell voltages of DBHFC decreased with the increasing of current density. The potential of DBHFC with Au/C as the anode catalyst decreased to 1.112 V rapidly when the current increased from 0 to 10 mA cm^{-2}. The large cell polarization could be due to the high overpotential of BH_4^- on Au surface. In the same condition, the potential of DBHFC with $Au_{80}Ni_{20}$/C and $Au_{58}Ni_{42}$/C as the anode catalyst decreased to 1.328 V and 1.356 V, respectively. This phenomenon exhibited that Au–Ni bimetallics can decrease overpotential of BH_4^- on Au surface and improve the performance of DBHFC. The cell performance using $Au_{41}Ni_{59}$/C as anode catalyst deteriorates rapidly, which is attributed to the seriously evolution of gaseous hydrogen at anode. It is found that DBHFC with

Table 4
Main performance parameters of the DBHFC using different anode catalysts.

DBHFC	Open circuit voltage OCP (V)	Current density, j (A cm^{-2})	Peak power density, P (mW cm^{-2})	Anode BH_4^- hydrolysis rate
Au/C	1.83	50	28.25	No significant bubbles
$Au_{80}Ni_{20}$/C	1.82	65	40.11	No significant bubbles
$Au_{58}Ni_{42}$/C	1.79	65	45.74	No significant bubbles
$Au_{41}Ni_{59}$/C	1.87	25	8.65	Abundant gas bubbles

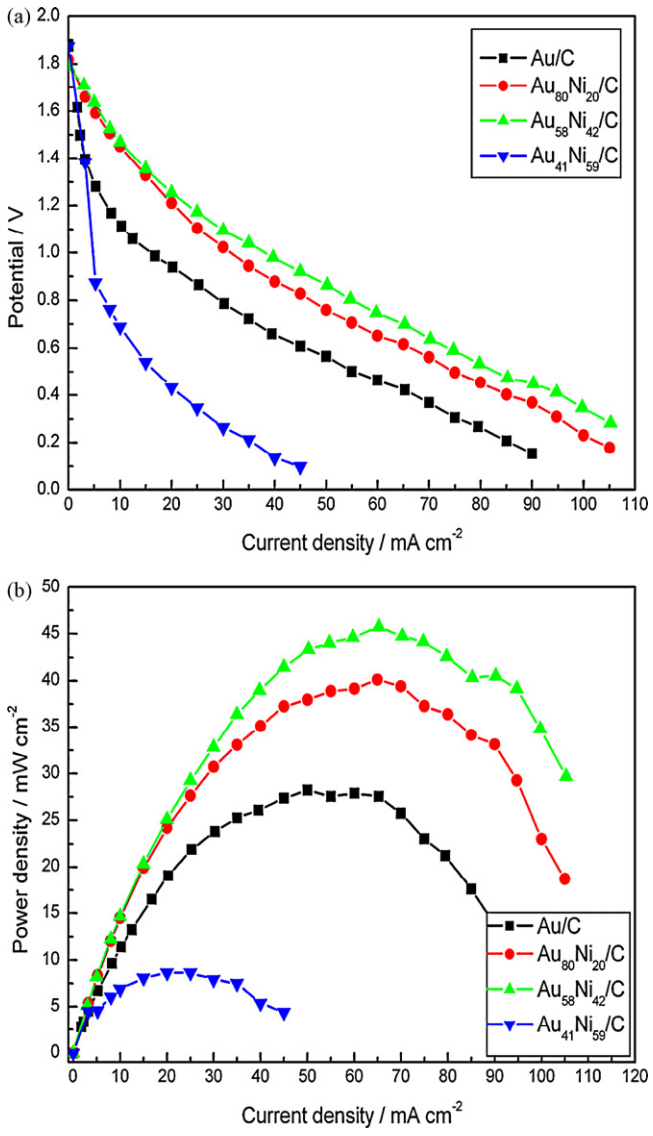

Fig. 7. The cell polarization and power density curves of the DBHFC using different anode catalysts at 20 °C with 1 M $NaBH_4$ + 3 M NaOH anolyte and 2 M H_2O_2 + 0.5 M H_2SO_4 catholyte. Catalyst loading: 4.5 mg cm^{-2}.

$Au_{58}Ni_{42}$/C as the anode catalyst give the best performance. The maximum power density is 45.74 mW cm^{-2} at a current density of 65 mA cm^{-2} at 20 °C.

4. Conclusions

In summary, the following conclusions can be made:

(1) Au–Ni bimetallic nanoparticles with different Au/Ni ratios were successfully prepared by a reverse micelle method. The catalyst particles were uniformly distributed throughout carbon black with regular spherical shape and narrow size distribution. The average size of the particles prepared was about 3 nm.

(2) Compared to Au/C catalyst, the oxidation peak potentials of BH_4^- on Au–Ni/C catalysts were about 0.15 V more negative, indicating that the Au–Ni bimetallic nanoparticles can apparently improve the catalytic activity of Au and the electrode kinetics of BH_4^- oxidation. The catalytic activity increased in the order of Au/C < $Au_{80}Ni_{20}$/C < $Au_{58}Ni_{42}$/C < $Au_{41}Ni_{59}$/C, but on $Au_{41}Ni_{59}$/C there was lots of gas bubble evolution.

(3) The direct borohydride-hydrogen peroxide fuel cell (DBHFC) using carbon supported Au–Ni bimetallic nanoparticles as anode was fabricated. It was found that the DBHFC using $Au_{58}Ni_{42}$/C as anode gave the best performance. The maximum power density was 45.74 mW cm^{-2} at 20 °C.

Therefore, the $Au_{58}Ni_{42}$/C bimetallic catalyst with high performance and low cost will be a promising anode catalyst for the application of DBFC.

Acknowledgments

This work was financially supported by the National Natural Science Foundation of China (Grant No. 20871101), Doctoral Fund of Ministry of Education of China (Grant No. 20094301110005) and Key Project of Educational Commission of Hunan Province, China (Grant No. 08A067).

References

[1] L.B. Wang, C.A. Ma, X.B. Mao, J.F. Sheng, F.Z. Bai, F. Tang, Electrochem. Commun. 7 (2005) 1477–1481.
[2] K. Deshmukh, K.S.V. Santhanam, J. Power Sources 159 (2006) 1084–1088.
[3] C. Ponce-de-Leon, D.V. Bavykin, F.C. Walsh, Electrochem. Commun. 8 (2006) 1655–1660.
[4] R.X. Feng, H. Dong, Y.D. Wang, X.P. Ai, Y.L. Cao, H.X. Yang, Electrochem. Commun. 7 (2005) 449–452.
[5] B.H. Liu, Z.P. Li, K. Arai, S. Suda, Electrochim. Acta 50 (2005) 3719–3725.
[6] G.H. Miley, N. Luo, J. Mather, R. Burton, G. Hawkins, L. Gu, E. Byrd, R. Gimlin, P.J. Shrestha, G. Benavides, J. Latstrom, D. Corroll, J. Power Sources 165 (2007) 509–516.
[7] R.K. Raman, S.K. Prashant, A.K. Shukla, J. Power Sources 162 (2006) 1073–1076.
[8] R.L. Pecsok, J. Am. Chem. Soc. 75 (1953) 2862–2864.
[9] M.E. Indig, R.N. Snyder, J. Electrochem. Soc. 109 (1962) 1104–1106.
[10] B.H. Liu, Z.P. Li, K. Arai, S. Suda, Electrochim. Acta 49 (2004) 3097–3105.
[11] E. Gyenge, M. Atwan, D. Northwood, J. Electrochem. Soc. 153 (2006) A150–A158.
[12] S.C. Amendola, P. Onnerud, M.T. Kelly, P.J. Petillo, S.L. Sharp-Goldman, M. Binder, J. Power Sources 84 (1999) 130–133.
[13] M.V. Mirkin, H. Yang, A.J. Bard, J. Electrochem. Soc. 139 (1992) 2212–2217.
[14] E. Gyenge, Electrochim. Acta 49 (2004) 965–978.
[15] J.H. Kim, H.S. Kim, Y.M. Kang, et al., J. Electrochem. Soc. 151 (2004) A1039–A1043.
[16] H.J. Wu, C. Wang, Z.X. Liu, Z.Q. Mao, Int. J. Hydrogen Energy 35 (2010) 2648–2651.
[17] H. Çelikkan, M. Şahin, M.L. Aksu, T.N. Veziroğlu, Int. J. Hydrogen Energy 32 (2007) 588–593.
[18] K.L. Wang, J.T. Lu, L. Zhuang, J. Phys. Chem. C 111 (2007) 7456–7462.
[19] M.H. Atwan, C.L.B. Macdonald, D.O. Northwood, E.L. Gyenge, J. Power Sources 158 (2006) 36–44.
[20] R.V. Malyala, C.V. Rode, M. Arai, S.G. Hegde, R.V. Chaudhari, Appl. Catal. A: Gen. 193 (2000) 71–86.
[21] J.L. Wei, X.Y. Wang, Y. Wang, J. Guo, P.Y. He, S.Y. Yang, N. Li, F. Pei, Y.S. Wang, Energy Fuels 23 (2009) 4037–4041.
[22] M.M. Maye, N.N. Kariuki, J. Luo, L. Han, P. Njoki, L. Wang, Y. Lin, H.R. Naslund, C.-J. Zhong, Gold Bull. 37 (2004) 217–233.
[23] A. Tegou, S. Armyanov, E. Valova, O. Steenhaut, A. Hubin, G. Kokkinidis, J. Electroanal. Chem. 634 (2009) 104–110.
[24] F. Hahn, B. Beden, M.J. Croissant, C. Lamy, Electrochim. Acta 31 (1986) 335–342.
[25] S.A.S. Machado, L.A. Avaca, Electrochim. Acta 39 (10) (1994) 1385–1391.
[26] B.E. Conway, L. Bai, J. Chem. Soc., Faraday Trans. I81 (1985) 1841.
[27] R. Woods, Electrochim. Acta 16 (1971) 655–659.
[28] S.E. Hörnström, L.I. Johansson, A. Flodström, Appl. Surf. Sci. 27 (1986) 235–246.
[29] M.Ø. Pedersen, S. Helveg, A. Ruban, I. Stensgaard, E. Laegsgaard, J.K. Nørskov, F. Besenbacher, Surf. Sci. 426 (1999) 395–409.
[30] N.A. Choudhury, R.K. Raman, S. Sampath, A.K. Shukla, J. Power Sources 143 (2005) 1–8.
[31] C. Ponce de león, F.C. Walsh, C.J. Patrissi, M.G. Medeiros, P.R. Bessette, R.W. Reeve, J.B. Lakeman, A. Rose, D. Browening, Electrochem. Commun. 10 (2008) 1610–1613.